Hexanuclear [Cp*Dy]₆ Single-Molecule Magnet

Jianfeng Wu, Serhiy Demeshko, Sebastian Dechert, and Franc Meyer*

General Synthetic Considerations. All chemicals and solvents were commercially obtained and used as received without any further purification, unless noted otherwise. THF and pentane were freshly distilled from Na and stored over molecular sieves. All the reactions and sample preparations were carried out in a glove box filled with dinitrogen. IR measurements of dried solid samples were performed inside an argon filled glovebox with a Cary 630 FTIR spectrometer equipped with Dial Path and Diamond ATR accessory and analyzed by FTIR MicroLab software. IR bands (Fig. S1) were labeled according to their relative intensities with vs (very strong), s (strong), m (medium), and w (weak). Elemental analyses of dried samples were carried out using an Elementar Vario EL III instrument by the analytical laboratory of the Institute of Inorganic Chemistry at the Georg-August-University Göttingen.

Magnetic Measurements. Magnetic susceptibility measurements were recorded on a Quantum-Design MPMS XL-5 SQUID magnetometer equipped with a 5 T magnet. The sample was prepared in a glove box filled with dinitrogen. Since the crystals gradually crumble after taking them out of the mother solution (which is attributed to the loss of solvent molecules), the fresh sample was quickly transferred into a capsule and covered with perfluoropolyether based inert oil Fomblin Y45 to prevent any loss of solvent molecules. The sample was then kept in a Schlenk flask and transferred into the SQUID magnetometer quickly. Direct current (dc) magnetic susceptibility measurements were performed on polycrystalline samples of **[Cp*Dy]₆** under an applied field of 5000 Oe, in the temperature range 2–210 K (below the pour point of the oil Fomblin Y45 to prevent any solvent loss and the reorientation of the sample under the applied field). Field-dependent magnetization was measured in the field range of 0−5 T. The dynamics of the magnetization were derived from ac susceptibility measurements under a 3.0 Oe oscillating ac field. Diamagnetic corrections were made with Pascal's constants[1] for all the constituent atoms as well as the contributions of the sample holder.

Synthesis of [Cp*Dy]₆. $DyCl_3$ (0.5 mmol) in 30 mL THF was stirred at room temperature overnight, then KCp* (0.5 mmol) in 10 mL THF was slowly added to the solution within 10 min. The reaction mixture was stirred at room temperature for 24 h and then filtered. The solvent was removed under vacuum and the residue was dissolved in THF. Slow diffusion of pentane into this solution gave yellow crystals of **[Cp*Dy]₆** suitable for X-ray diffraction after one week. Yield: 580 mg, (40%, based on metal salt). Elemental analysis (%) for dried material of $[(Cp*Dy)_6K_4Cl_{16}(THF)_6]$ ($C_{84}H_{138}Cl_{16}Dy_6K_4O_6$, MW = 2942.54): calcd C, 30.77, H, 4.03 (after loss four THF); found C, 30.55, H, 4.01. IR (solid, ATR) $\tilde{v}$ [cm⁻¹] = 2973 (w), 2898 (s), 2857 (m), 1449 (s), 1379 (m), 1250 (m), 1014 (s), 914 (w), 855 (vs), 800 (m), 668 (w), 541 (m).
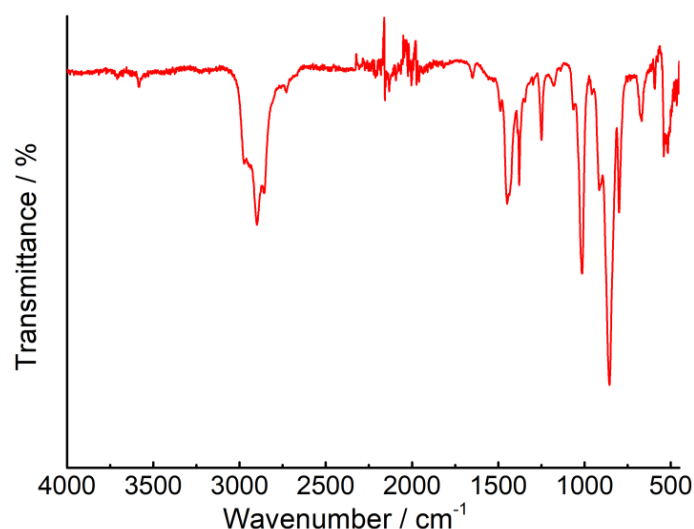
Fig. S1 IR(ATR) spectrum of a solid sample of **[Cp*Dy]₆**.

X-ray crystallography. Crystal data and details of the data collections are given in Table S1. X-ray data were collected on a STOE IPDS II diffractometer (graphite monochromated Mo-Kα radiation, λ = 0.71073 Å) by use of ω scans at –140 °C. The structure was solved with SHELXT and refined on F^2 using all reflections with SHELXL-2018.[2] Non-hydrogen atoms were refined anisotropically. Hydrogen atoms were placed in calculated positions and assigned to an isotropic displacement parameter of 1.2/1.5 U_{eq}(C). The asymmetric unit contains one and a half molecule which results in an overall Z=3. Two THF solvent molecules were found to be disordered about two positions (occupancy factors: 0.62(3) / 0.38(3) & 0.646(16) / 0.354(16)) and were refined using SAME, DELU and RIGU restraints. Face-indexed absorption corrections were performed numerically with the program X-RED.[3] CCDC 1972215 contains the supplementary crystallographic data for this paper. These data can be obtained free of charge from the Cambridge Crystallographic Data Centre via www.ccdc.cam.ac.uk/data_request/cif.

Table S1. Crystallographic data of complex **[Cp*Dy]₆**.

	[Cp*Dy]₆
empirical formula	$C_{84}H_{138}Cl_{16}Dy_6K_4O_6$
formula weight, g·mol⁻¹	2942.54
crystal size, mm³	0.50 x 0.41 x 0.36
crystal system	Triclinic
space group	P–1
T, K	133(2)
$λ$, Å	0.71073
a, Å	13.9788(2)
b, Å	16.4794(2)
c, Å	37.2813(6)
$α$, °	85.933(1)
$β$, °	84.334(1)

γ, °	70.868(1)
V, Å^3	8067.4(2)
Z	3
ρ (cal), g·cm^{-3}	1.817
F(000)	4302
θ range [°]	1.099 to 25.693
Tmax / Tmin	0.3283 / 0.1681
measured refl.	94553
unique refl. [Rint]	30247, 0.0314
goodness-of-fit (F^2)	1.049
data / restr. / param.	30247 / 260 / 1704
$R1$, $wR2$ ($I > 2\sigma(I)$)	0.0372, 0.0982
$R1$, $wR2$ (all data)	0.0439, 0.1059
res. el. dens. [e·Å^{-3}]	1.028 / −2.283
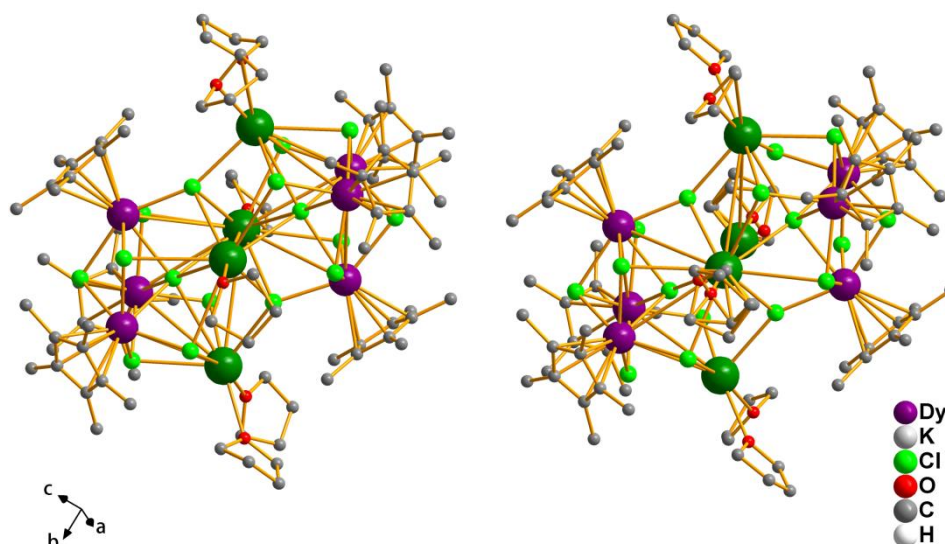
Fig. S2 Solid state structure of **[Cp*Dy]₆**; hydrogen atoms are omitted for clarity.
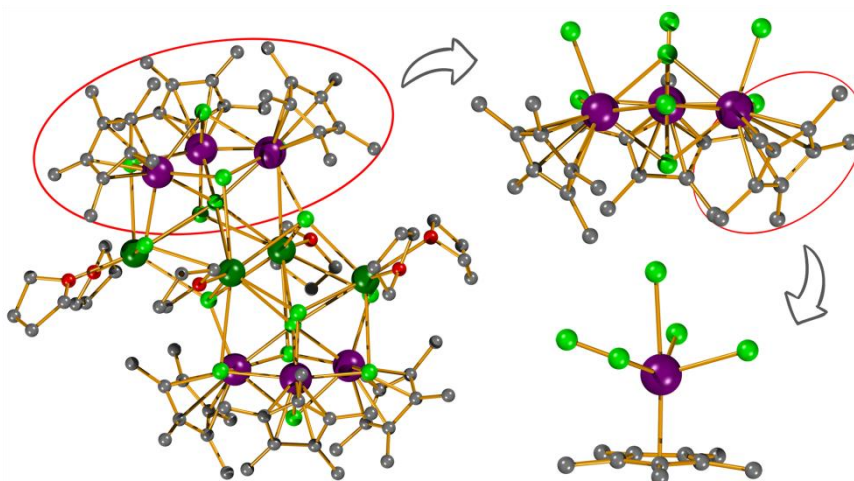
Fig. S3 Structure view of complex **[Cp*Dy]₆**; hydrogen atoms are omitted for clarity. On the right fragments are shown to illustrate the (Cp*Dy)₃ subunits and the coordination of an individual Dy^{III} ion.
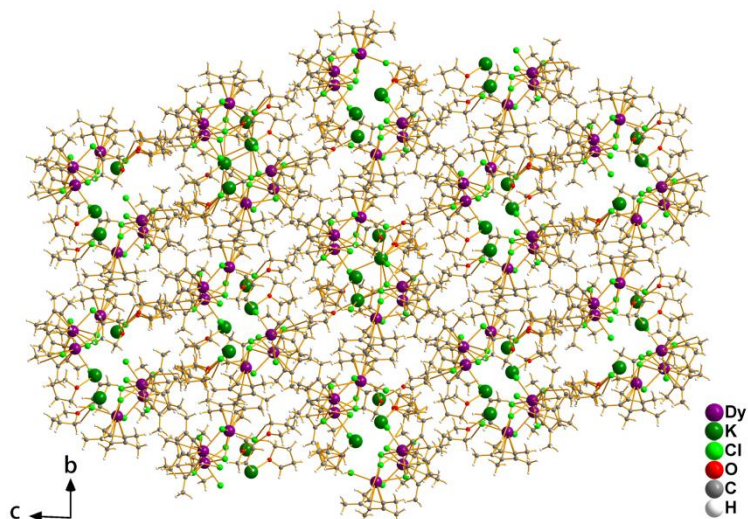
Fig. S4 Packing model of complex **[Cp*Dy]₆** along the crystallographic *a* axis.
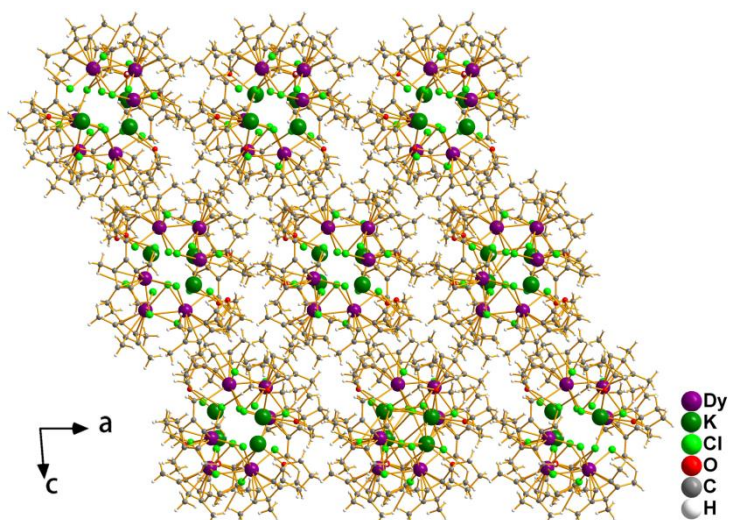
Fig. S5 Packing model of complex **[Cp*Dy]₆** along the crystallographic *b* axis.
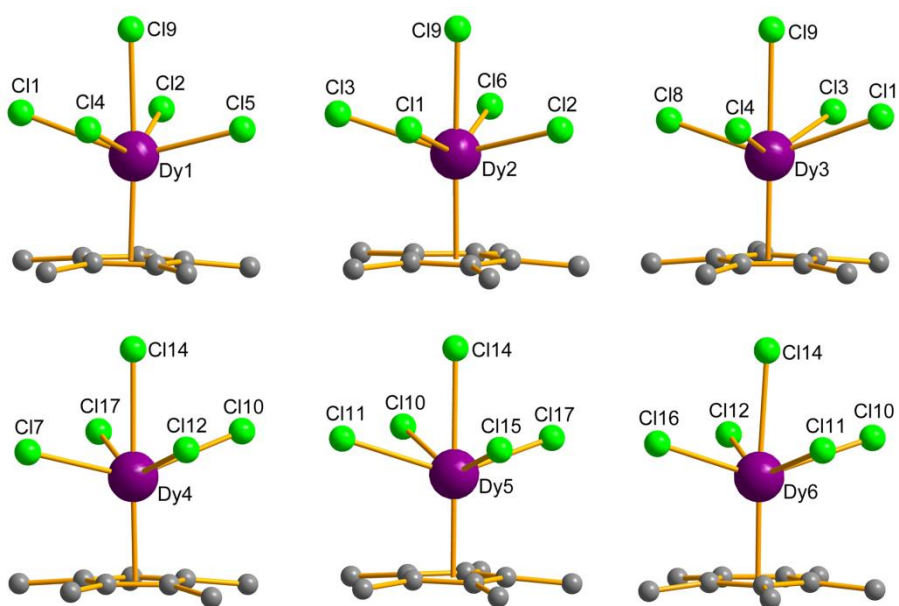
Fig. S6 Coordination environments of each Dy^{III} ion in **[Cp*Dy]₆**.

Table S2. Selected bond distances (Å) in **[Cp*Dy]₆**.

Dy(1)-Cl(5)	2.6421(13)	Dy(2)-Cl(6)	2.6068(13)	Dy(3)-Cl(8)	2.6024(14)
Dy(1)-Cl(4)	2.7200(13)	Dy(2)-Cl(2)	2.7388(13)	Dy(3)-Cl(4)	2.7349(13)
Dy(1)-Cl(2)	2.7241(13)	Dy(2)-Cl(3)	2.7724(14)	Dy(3)-Cl(3)	2.7637(13)
Dy(1)-Cl(1)	2.8118(13)	Dy(2)-Cl(9)	2.8113(13)	Dy(3)-Cl(9)	2.8489(12)
Dy(1)-Cl(9)	2.8382(12)	Dy(2)-Cl(1)	2.8953(12)	Dy(3)-Cl(1)	2.8768(14)
Dy(1)-Cp*(1)	2.3428(5)	Dy(2)-Cp*(2)	2.3375(3)	Dy(3)-Cp*(3)	2.3412(6)
Dy(4)-Cl(7)	2.6077(13)	Dy(5)-Cl(15)	2.6061(13)	Dy(6)-Cl(16)	2.6168(13)
Dy(4)-Cl(12)	2.7072(13)	Dy(5)-Cl(17)	2.7363(13)	Dy(6)-Cl(12)	2.7323(13)
Dy(4)-Cl(17)	2.7314(13)	Dy(5)-Cl(11)	2.7584(13)	Dy(6)-Cl(11)	2.7539(13)
Dy(4)-Cl(10)	2.8063(13)	Dy(5)-Cl(14)	2.8403(13)	Dy(6)-Cl(14)	2.8401(12)
Dy(4)-Cl(14)	2.8575(12)	Dy(5)-Cl(10)	2.8873(12)	Dy(6)-Cl(10)	2.8630(13)
Dy(4)-Cp*(4)	2.3360(5)	Dy(5)-Cp*(5)	2.3391(3)	Dy(6)-Cp*(6)	2.3400(7)

Table S3. Selected bond angles (°) in **[Cp*Dy]₆**.

Cp*(1)-Dy(1)-Cl(5)	106.387(32)	Cp*(2)-Dy(2)-Cl(6)	106.354(34)	Cp*(3)-Dy(3)-Cl(8)	104.957(37)
Cp*(1)-Dy(1)-Cl(4)	106.574(31)	Cp*(2)-Dy(2)-Cl(2)	104.730(28)	Cp*(3)-Dy(3)-Cl(4)	106.325(30)
Cp*(1)-Dy(1)-Cl(2)	107.936(32)	Cp*(2)-Dy(2)-Cl(3)	107.511(32)	Cp*(3)-Dy(3)-Cl(3)	107.277(31)
Cp*(1)-Dy(1)-Cl(1)	106.831(29)	Cp*(2)-Dy(2)-Cl(1)	107.861(29)	Cp*(3)-Dy(3)-Cl(1)	110.489(29)
Cp*(1)-Dy(1)-Cl(9)	176.808(31)	Cp*(2)-Dy(2)-Cl(9)	176.143(29)	Cp*(3)-Dy(3)-Cl(9)	178.578(31)
Cp*(4)-Dy(4)-Cl(7)	104.746(38)	Cp*(5)-Dy(5)-Cl(15)	106.332(34)	Cp*(6)-Dy(6)-Cl(16)	107.980(31)
Cp*(4)-Dy(4)-Cl(12)	105.886(31)	Cp*(5)-Dy(5)-Cl(17)	105.430(31)	Cp*(6)-Dy(6)-Cl(12)	105.185(29)
Cp*(4)-Dy(4)-Cl(17)	108.221(32)	Cp*(5)-Dy(5)-Cl(11)	107.574(30)	Cp*(6)-Dy(6)-Cl(11)	107.154(32)
Cp*(4)-Dy(4)-Cl(10)	108.735(29)	Cp*(5)-Dy(5)-Cl(10)	107.562(29)	Cp*(6)-Dy(6)-Cl(10)	106.435(28)
Cp*(4)-Dy(4)-Cl(14)	178.805(31)	Cp*(5)-Dy(5)-Cl(14)	176.703(29)	Cp*(6)-Dy(6)-Cl(14)	176.068(31)
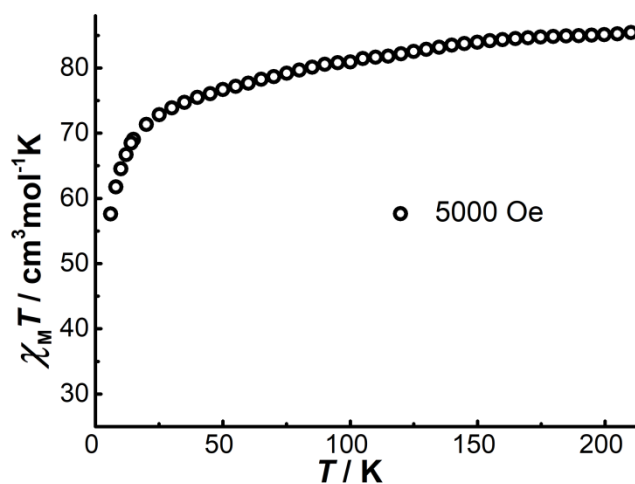
Fig. S7 Temperature dependence of the $\chi_M T$ product for **[Cp*Dy]₆** at 5 kOe between 2 and 210 K.
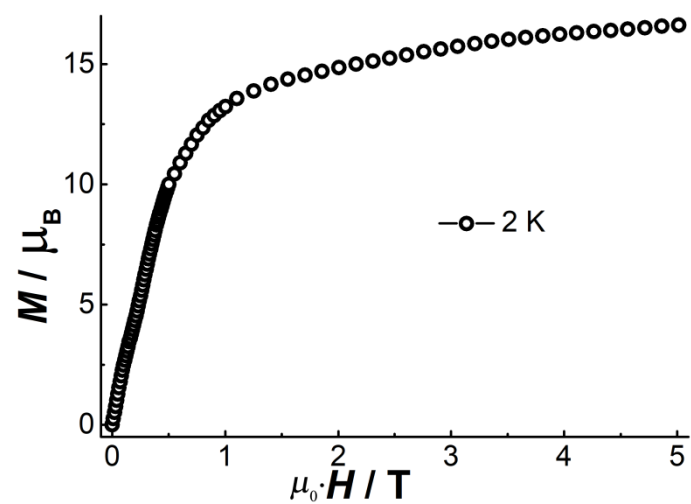
Fig. S8 Plot of the molar magnetization (*M*) *vs.* field (*H*) for **[Cp*Dy]$_6$** at 2.0 K.
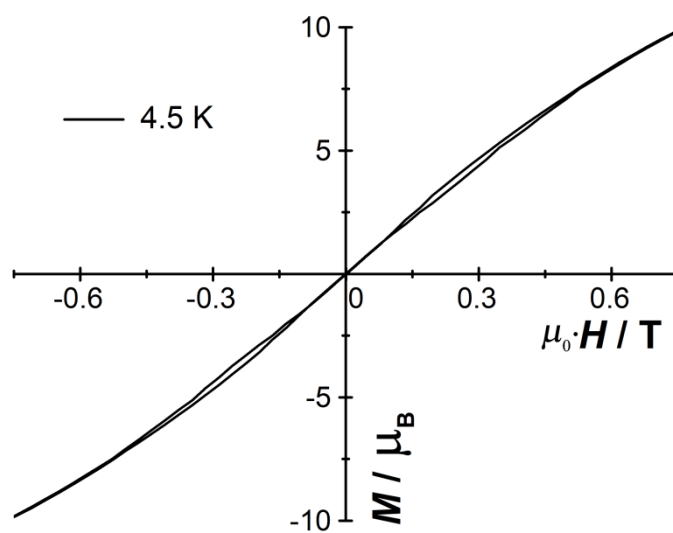
Fig. S9 Magnetic hysteresis of **[Cp*Dy]$_6$** at 4.5 K with a sweep rate of 0.002 T·s^{-1}.
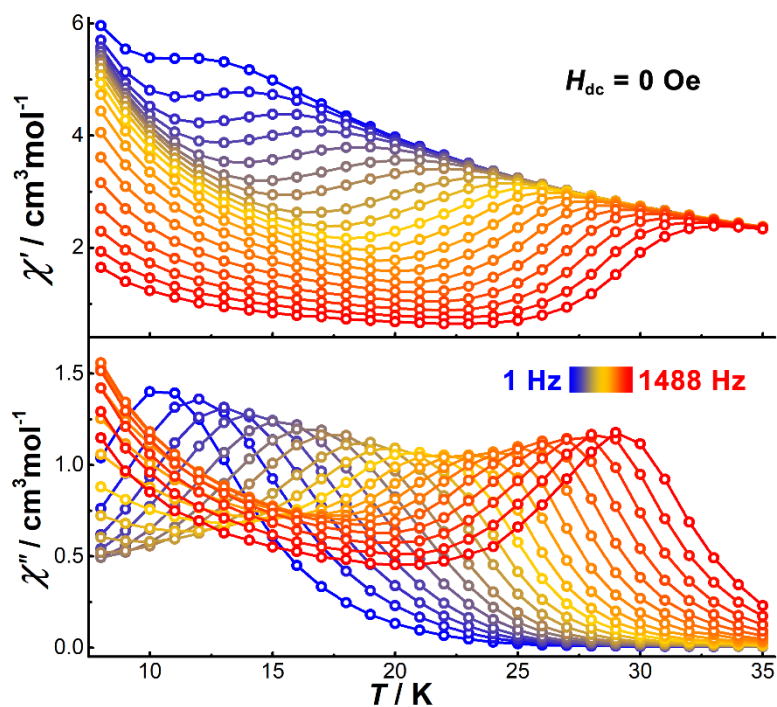
Fig. S10 Temperature-dependence of the in-phase (top) and out-of-phase (bottom) parts of the ac susceptibility for [Cp*Dy]₆ under zero dc field.
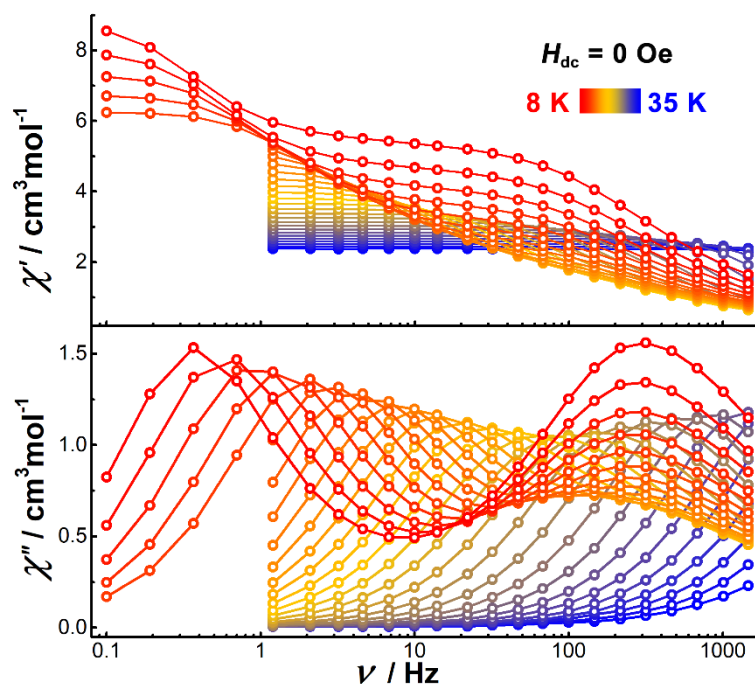
Fig. S11 Frequency-dependence of the in-phase (top) and out-of-phase (bottom) parts of the ac susceptibility for [Cp*Dy]₆ under zero dc field in the indicated temperature range.
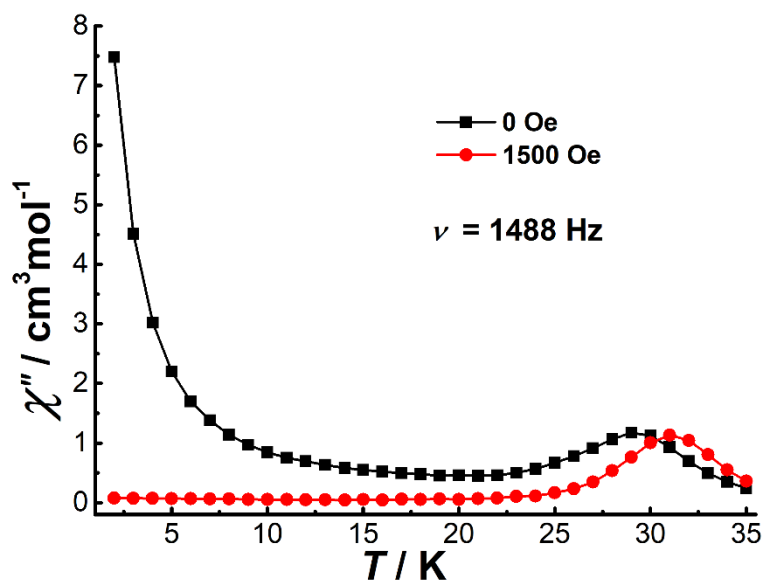
Fig. S12 Temperature-dependence of the out-of-phase parts of the ac susceptibility for **[Cp*Dy]₆** under zero and 1500 Oe dc field at the indicated frequency.
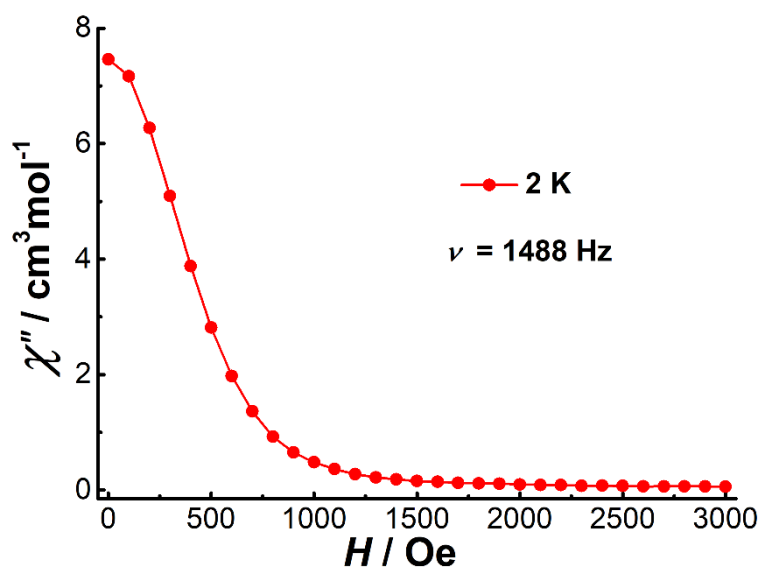
Fig. S13 Field-dependence of the out-of-phase parts of the ac susceptibility for **[Cp*Dy]₆** at 2 K and at the indicated frequency.
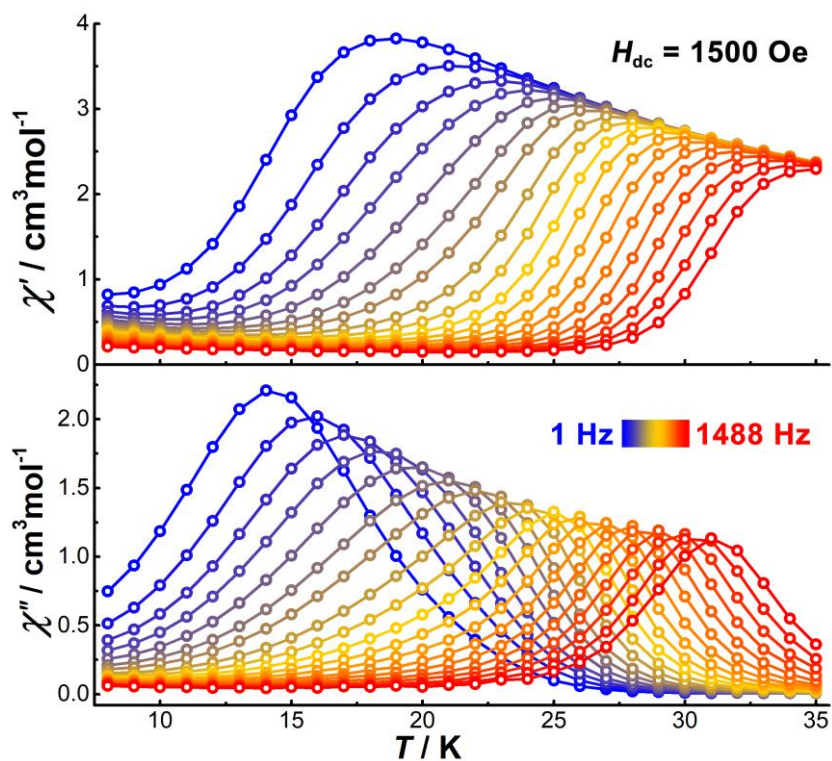
Fig. S14 Temperature-dependence of the in-phase (top) and out-of-phase (bottom) parts of the ac susceptibility for **[Cp*Dy]₆** under 1500 Oe dc field.
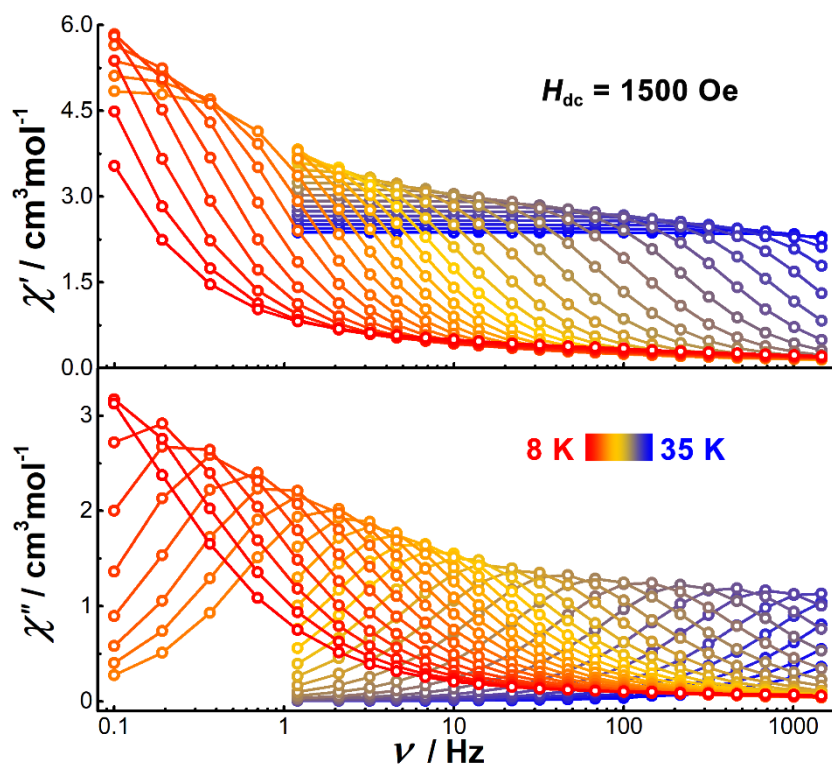
Fig. S15 Frequency-dependence of the in-phase (top) and out-of-phase (bottom) parts of the ac susceptibility of **[Cp*Dy]₆** under 1500 Oe dc field in the indicated temperature range.
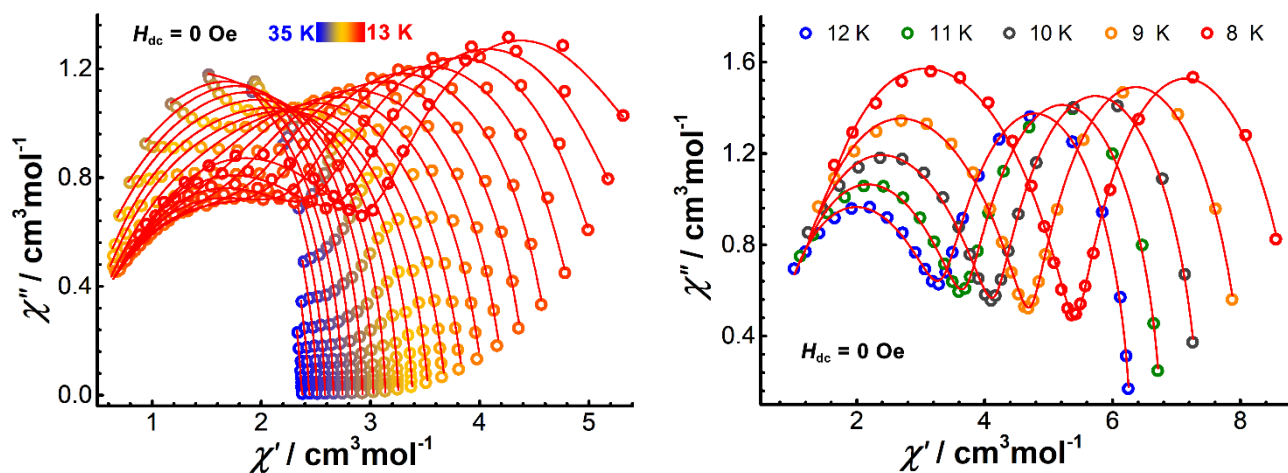
Fig. S16 Cole-Cole plots for **[Cp*Dy]₆** under zero dc field in the temperature range 35–13 K (left) and 12–8 K (right); the red lines represent the best fits in the indicated temperature range.
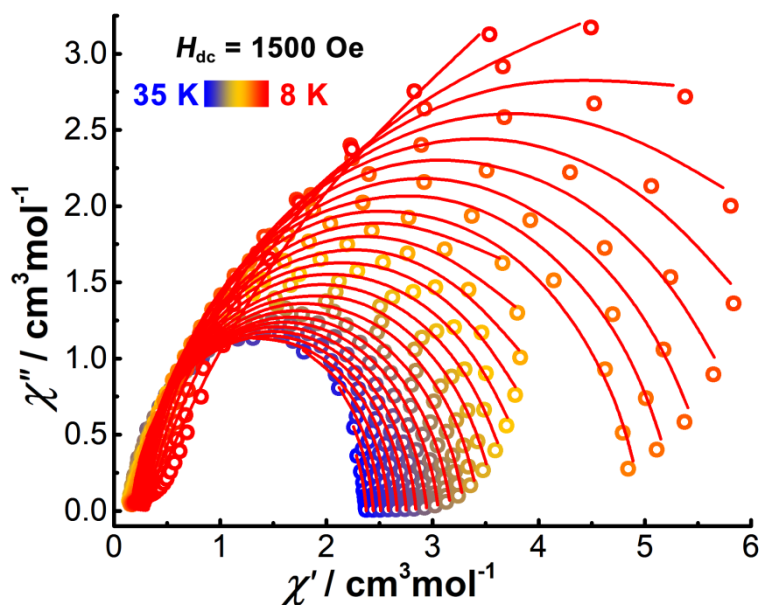
Fig. S17 Cole-Cole plots for **[Cp*Dy]₆** under 1500 Oe dc field; the red lines represent the best fits in the indicated temperature range.

Table S4. Parameters for the best fit of frequency-dependent ac susceptibility of **[Cp*Dy]₆** under zero dc field.

T / K	$\chi_{S,tot}$	$\Delta\chi_1$	τ_1 / s	α_1	$\Delta\chi_2$	τ_2 / s	α_2	Residual
32		5.39162	1.68374E-5	0.10305				8.31008E-6
31		3.08407	3.67933E-5	0.07023				8.87294E-6
30		2.51364	7.22835E-5	0.03879				1.15972E-5
29		2.49741	1.24728E-4	0.03463				8.70667E-6
28		2.5516	2.26236E-4	0.04627				2.71921E-5
27		2.6948	3.89534E-4	0.08492				2.43887E-4
26	0.52873	1.91119	6.02758E-4	0.03067	0.8984	1.40142E-4	0.25367	1.56638E-5
25	0.42685	0.48683	0.00124	0.01447	2.5048	4.7493E-4	0.17752	6.70953E-4
24	0.44577	0.91937	0.00197	0.01753	2.1865	5.00984E-4	0.20394	1.74864E-4
23	0.46005	1.2373	0.00281	0.01185	2.01644	5.14528E-4	0.23059	1.94349E-4
22	0.58974	1.58292	0.00362	0.05759	1.83081	5.16598E-4	0.27548	3.2128E-4
21	0.40449	1.77336	0.00486	0.0689	1.83443	5.13697E-4	0.32229	3.60438E-4
20	0.32971	1.84802	0.00676	0.05761	1.98335	5.09462E-4	0.3628	2.59973E-4
19	0.27289	1.89171	0.0094	0.04063	2.16855	5.17441E-4	0.39103	1.42651E-4
18	0.27229	1.95337	0.01294	0.02883	2.34161	5.1773E-4	0.40486	9.34926E-5
17	0.37808	2.10568	0.01753	0.03067	2.36181	5.1219E-4	0.38051	7.2799E-5
16	0.39851	2.31769	0.02325	0.04329	2.36046	5.07367E-4	0.34587	5.7222E-5
15	0.46365	2.45047	0.03152	0.0477	2.48655	5.08097E-4	0.33081	4.9487E-5
14	0.4843	2.56133	0.04266	0.0501	2.66213	4.88758E-4	0.32546	7.28561E-5
13	0.52123	2.68465	0.05978	0.05154	2.86439	5.04103E-4	0.31383	1.01307E-4
12	0.53846	2.76905	0.08485	0.04452	3.16652	5.12665E-4	0.31588	1.53336E-4
11	0.61275	2.91587	0.12121	0.05116	3.42517	5.18624E-4	0.30122	1.55327E-4
10	0.67208	3.04976	0.17973	0.05549	3.82768	5.1716E-4	0.29549	2.56541E-4
9	0.74815	3.20203	0.26992	0.06311	4.26265	5.1789E-4	0.2822	4.28128E-4
8	0.90458	3.36542	0.422	0.07445	4.85943	5.177E-4	0.2692	0.00145

Table S5. CC-Fit[4] results for frequency-dependent ac susceptibility of **[Cp*Dy]₆** under 1500 Oe dc field.

T / K	χ_S	χ_T	τ / s	α	Residual
8	0.31368	13.864	4.47334	0.31444	0.13852
9	0.30178	9.95272	2.11347	0.24529	0.13099
10	0.29099	8.23269	1.04954	0.19342	0.12757
11	0.27524	7.25643	0.60791	0.1602	0.11909
12	0.26111	6.58377	0.38292	0.13805	0.10603
13	0.24687	6.05548	0.24976	0.12366	0.08682
14	0.23424	5.61966	0.16825	0.11308	0.07055
15	0.22207	5.27805	0.11923	0.10672	0.05795
16	0.20954	4.96514	0.08495	0.10214	0.04788
17	0.18751	4.877	0.06605	0.12415	0.01677
18	0.18096	4.5847	0.04807	0.11755	0.01458
19	0.17544	4.33611	0.03557	0.11321	0.01351
20	0.16978	4.12197	0.02644	0.11211	0.01333
21	0.16493	3.92695	0.01945	0.11119	0.01406
22	0.163	3.75239	0.01391	0.11109	0.01376
23	0.1601	3.5899	0.00946	0.11071	0.016
24	0.15619	3.43823	0.00604	0.1082	0.01411
25	0.15488	3.299	0.00364	0.10393	0.01397
26	0.15403	3.17063	0.00209	0.09738	0.01235
27	0.15329	3.05358	0.00118	0.08908	0.01083
28	0.14949	2.94553	6.53365E-4	0.08126	0.00934
29	0.162	2.84331	3.66501E-4	0.07085	0.00564
30	0.18024	2.75075	2.11445E-4	0.05893	0.0037
31	0.18304	2.66478	1.23421E-4	0.05169	0.00165
32	0.16963	2.58431	7.33894E-5	0.04635	9.32344E-4
33	0.01009	2.5105	4.11299E-5	0.05343	5.50785E-4
34	0.059388	2.44094	2.52888E-5	0.05202	8.81117E-4
35	0.0826041	2.37567	1.57264E-5	0.05881	0.0011

Table S6. Parameters obtained from the fitting of the plots of relaxation time (τ) *vs.* $1/T$ for **[Cp*Dy]$_6$**.

		U_{eff} / K	τ_0 / s	τ_{QTM} / s	C / s^{-1} K^{-n}	n	Residual
0 Oe	SR	454	1.7E-11	2.1	1.8E-4	4.4	8.55E-7
	FR	--	--	5.1 E-4	--	--	7.02E-11
1500 Oe		561	1.3E-12	--	2.0E-6	5.6	3.98 E-5
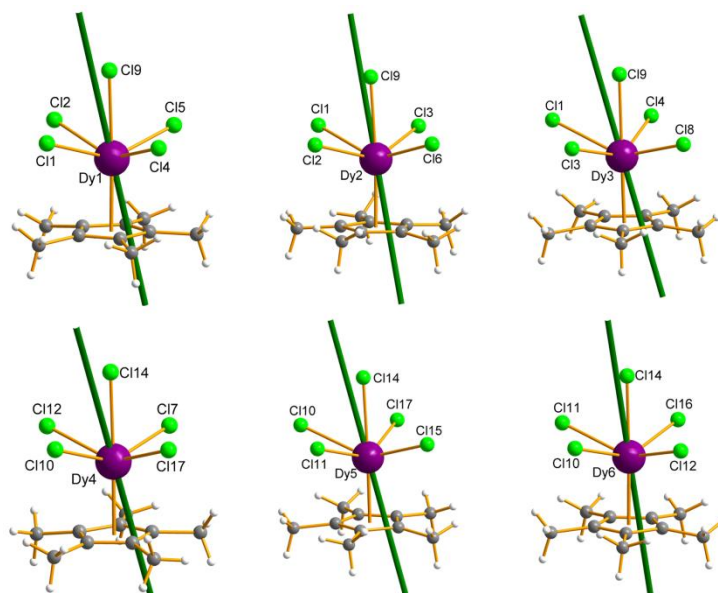
Fig. S18 Orientations of the main magnetic axis of the ground state for each Dy^{III} ion of **[Cp*Dy]$_6$**, calculated based on single ion coordination.
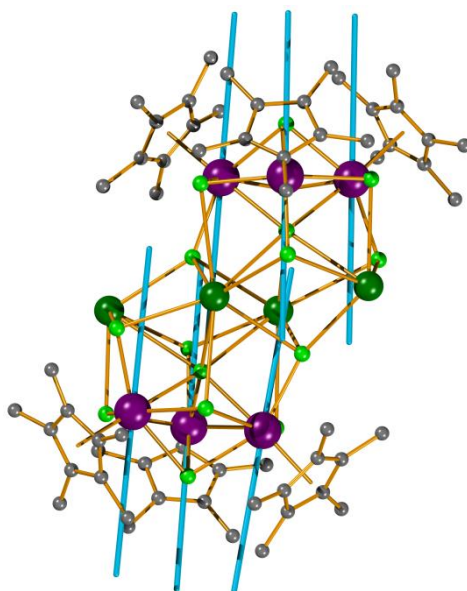
Fig. S19 Orientations of the main magnetic axes for the ground state of **[Cp*Dy]$_6$** calculated based on the entire molecule. The coordinated THF have been omitted for clarity.

Table S7. Minimal reorientation energies (cm^{-1}) and intersection angles (°) of anisotropy axes of **[Cp*Dy]$_6$** calculated using the Magellan program.[5]

Site	Optimized energy (cm^{-1})	Min. reversal energy (cm^{-1})	Intersection angles (°)
Dy1	-0.1846E+03	0.1121E+03	0
Dy2	-0.2258E+03	0.2336E+03	6.698
Dy3	-0.1945E+03	0.1710E+03	5.813
Dy4	-0.1922E+03	0.1204E+03	7.529
Dy5	-0.2022E+03	0.2053E+03	13.752
Dy6	-0.2312E+03	0.2028E+03	9.07

References:

1 E. A. Boudreaux and L. N. Mulay, *Theory and Applications of Molecular Paramagnetism*, John Wiley & Sons,: New York, 1976.

2 a) G. Sheldrick, *Acta Cryst. A*, 2015, **71**, 3; b) *Acta Cryst. C*, 2015, **71**, 3.

3 *X-RED*, STOE & CIE GmbH, Darmstadt, Germany, 2002.

4 D. Reta and N. F. Chilton, *ChemRxiv*, 2019, 10.26434/chemrxiv.8863904.v1.

5 N. F. Chilton, D. Collison, E. J. L. McInnes, R. E. P. Winpenny and A. Soncini, *Nat. Commun.*, 2013, **4**, 2551.